Competition Between Supernucleation and Plasticization in the Crystallization and Rheological Behavior of PCL/CNT-Based Nanocomposites and Nanohybrids

Juan F. Vega,[1] Joel Fernández-Alcázar,[1] Juan V. López,[2] Rose Mary Michell,[2] Ricardo A. Pérez-Camargo,[3] Benoit Ruelle,[4] Javier Martínez-Salazar,[1] María Luisa Arnal,[2] Philippe Dubois,[4] Alejandro J. Müller[2,3,5]

[1]BIOPHYM, Departamento de Física Macromolecular, Instituto de Estructura de la Materia (IEM-CSIC), Serrano 113 bis, Madrid 28006, Spain
[2]Grupo de Polímeros USB, Departamento de Ciencia de los Materiales, Universidad Simón Bolívar, Apartado 89000, Caracas 1080-A, Venezuela
[3]POLYMAT and Polymer Science and Technology Department, Faculty of Chemistry, University of the Basque Country UPV/EHU, Paseo Manuel de Lardizabal 3, Donostia-San Sebastián 20018, Spain
[4]Service des Matériaux Polymères et Composites SMPC, Center of Research and Innovation in Materials & Polymers CIRMAP, Université de Mons-UMONS, Place du Parc 20, Mons B-7000, Belgium
[5]IKERBASQUE, Basque Foundation for Science, Bilbao, Spain
Correspondence to: A. J Müller (E-mail: alejandrojesus.muller@ehu.es)

Received 27 March 2017; accepted 22 May 2017; published online 14 June 2017
DOI: 10.1002/polb.24385

ABSTRACT: PCL was blended with pristine multiwalled carbon nanotubes (MWCNT) and with a nanohybrid obtained from the same MWCNT but grafted with low molecular weight PCL, employing concentrations of 0.25 to 5 wt % of MWCNT and MWCNT-*g*-PCL. Excellent CNT dispersion was found in all samples leading to supernucleation of both nanofiller types. Nanohybrids with 1 wt % or less MWCNTs crystallize faster than nanocomposites (due to supernucleation), while the trend eventually reverses at higher nanotubes content (because of plasticization). Rheological results show that yield-like behavior develops in both nanocomposites, even for the minimum content of carbon nanotubes. In addition, the MWCNT-*g*-PCL family, when compared with the neat polymer, exhibits lower values of viscosity and modulus in oscillatory shear, and higher compliance in creep. These rheological differences are discussed in terms of the plasticization effect caused by the existence of low molecular weight free and grafted PCL chains in the nanohybrids. © 2017 Wiley Periodicals, Inc. J. Polym. Sci., Part B: Polym. Phys. **2017**, *55*, 1310–1325

KEYWORDS: crystallization; differential scanning calorimetry (DSC); nanocomposites; rheology

INTRODUCTION Nanocomposites are highly attractive materials, as the inclusion of nanofillers in polymers leads to an improvement in several mechanical and electrical properties. Carbon nanotubes (CNT)s are one of the most commonly employed conductive nanofillers, as they have an exceptionally large aspect ratio and low density, which makes them ideal for blending with polymeric materials. In these blends, the obtained materials exhibit a good balance between lightness and outstanding properties, which are ideal for nanotechnology.[1–6]

The nanocomposites of poly(ε-caprolactone) (PCL) with CNT have potential applications in the biodegradable packaging market and in the biomedical field since the presence of the CNTs could overcome disadvantages of PCL with respect to mechanical properties and thermal stability.[4,7–15]

Several studies deal with the incorporation of CNTs to PCL, and they have found that CNTs could improve biodegradation rate,[9,16] mechanical performance,[17–19] thermal stability, and nucleate PCL.[9,11,18–24] Additionally, an electric percolation threshold in a range of 0.08–3 wt % has been reported.[23–25]

The influence of CNTs on the viscoelastic properties of polymers has also been a subject of great interest in the last decades. The presence of fillers of any type in polymeric matrices leads to a well-known hydrodynamic reinforcement at low filler concentration.[26] In this dilute regime, particle–particle

Additional Supporting Information may be found in the online version of this article.

interactions are screened, and the changes in the properties depend on the nature of the interface between the particles and the polymeric matrix. At a given concentration, that is, the percolation threshold, the fillers form a network, which is responsible for the development of yield points and solid-like behavior.[3,27–32] Moreover, the composition at which the transition from liquid-like to solid-like behavior occurs is an indication of the quality of the distribution and dispersion of the nanofiller throughout the matrix, the interaction between the filler particles and the matrix, or the filler aspect ratio and/or orientation.

Hence, different values of the percolation threshold can be found in the literature for several types of nanocomposites based on PCL and CNTs. For systems prepared by dispersion of the CNTs in PCL matrices with the aid of solvents, values of the rheological threshold in the range 0.07–0.7 wt % have been found.[25,33] For systems obtained by melt blending, much higher values around 0.3–3 wt % have been reported.[24,34,35]

In this work, we compare the influence on the crystallization and rheological properties of two kinds of nanocomposites obtained by the incorporation of modified (i.e., CNT surface-grafted with PCL) and unmodified CNT to a PCL matrix with compositions ranging from 0.25 to 5 wt %. Additionally, the effect of the low molecular weight PCL chains produced during the CNT modification on the crystallization and rheological properties is also examined.

EXPERIMENTAL

Materials

The poly(ε-caprolactone) (CAPA 6500) was a commercial sample produced by Solvay interox, with a number average molecular weight of 50,000 g/mol. Two types of CNT were employed, functionalized and nonfunctionalized Multiwall Carbon Nanotubes (MWCNT). The industrial grade NC7000 was produced by Nanocyl (Sambreville, Belgium). The method of synthesis was catalytic carbon vapor deposition (CCVD), the average diameter is 10 nm, and their average length is around 2 μm. They contain less than 10 wt % of metal oxide impurities that remain from the catalyst and catalytic support.

In a first step, the MWCNTs were modified by exposing them to a flow of atomic nitrogen (provided from an $Ar + N_2$ microwave plasma)[36] and molecular hydrogen. These functionalized MWCNTs present a grafting of 1 at.% of nitrogen group whose 70% are primary amines groups.[37]

The MWCNT-*g*-PCL nanohybrids were prepared by ROP of ε-CL initiated by primary amine groups grafted onto the MWCNTs and catalyzed by $AlEt_3$. ε -caprolactone (ε-CL, 99%, Fluka) was dried over calcium hydride (93 + %, Acros) for 48 h and, then, distilled under reduced pressure and kept under nitrogen at 4 °C. The triethylaluminum solution ($AlEt_3$, 25 wt % in toluene, Aldrich) was diluted in dried toluene to obtain a 1 M solution, which was stored under nitrogen atmosphere. The MWCNT-*g*-PCL nanohybrids were prepared by ROP of ε-CL initiated by primary amine groups grafted onto the MWCNTs (0.5 g) by the addition of 1 mL of $AlEt_3$ (1 M) and, then 4 mL of ε-CL (4.12 g). The ROP of ε-CL occurred for 24 h, and the reaction system became viscous suggesting that the polymerization took place. The reaction medium was poured in a large excess of heptane to selectively precipitate the PCL-grafted MWCNTs and any "free" (non-grafted) PCL that could be formed directly in solution via homogeneous initiation from hydroxyl impurities present in the medium. After drying, the obtained gray powder contained a mixture of MWCNT-*g*-PCL nanohybrids and "free" PCL chains which could be removed by washing the product with toluene via Soxhlet extraction for 1 day. After Soxhlet extraction of "free" PCL chains with toluene, we determined by TGA analyses that the composition of MWCNT-*g*-PCL + "free" PCL chains sample is: 20 wt % of MWCNTs, 7 wt % of grafted PCL, and 73 wt % of "free" PCL.

To determine the number-average molecular weight (M_n) of grafted polymer chains, the common strategy consists in breaking the bonds between MWCNTs and the grafted polymer and to analyze the so-formed homopolymer by Gel Permeation Chromatography (GPC).[38] However, this strategy cannot be used to characterize our samples because the polymer chains are linked via a covalent amide bond at the MWCNT surface, and amide bonds are known to be more stable than ester bonds of PCL. Nevertheless, by GPC, we determined the number average molecular weight (M_n) of "free" PCL chains to be equal to 12,000 g/mol with a dispersity ($Đ$) of 2.1. Therefore, knowing the quantity of PCL chains covalently grafted per gram of MWCNTs and the primary amine content per gram of MWCNTs, assuming that each NH_2 groups effectively participates in the initiation of ε-CL polymerization, the number average molecular weight of grafted PCL chains can be estimated to be 500–1000 g/mol (see ref. 37). This value is lower than the entanglement molecular weight, $M_e = 3000$ g/mol, reported for PCL.[39]

Thus, the final weight composition of the PCL sample filled with MWCNT-*g*-PCL + PCL (3 wt % of MWCNTs) was 3 wt % of MWCNTs, 1 wt % of grafted PCL, 11 wt % of "free" low molecular weight PCL chains and 85 wt % of the high molecular weight PCL matrix (CAPA6500).

The PCL (i.e., CAPA 6500) was blended with 0.25, 0.3, 0.5, 0.75, 1, 2, and 3% w/w of the previously prepared MWCNT-*g*-PCL (i.e., nanohybrids) and up to 5% w/w of nonfunctionalized MWCNT (i.e., nanocomposites), respectively. Table 1 reports the sample nomenclature (i.e., M refers to unmodified MWCNT and NH refers to nanohybrid and corresponds to the modified MWCNT (MWCNT-*g*-PCL) employed in this work.

Morphological Evaluation (TEM)

The morphological observations were performed by Transmission Electron Microscopy (TEM) with a TECNAI G2 20 TWIN (FEI) microscope, operating at an accelerating voltage of 200 kV in bright-field image mode. The samples, which are films, were sectioned using a Leica EMFC 6

TABLE 1 Characteristics and Nomenclature of the Materials Employed

Name	MWCNT (% wt)	*g*-PCL (wt %)	Free PCL (wt %)	Matrix PCL (wt %)	Total PCL (% wt)
PCL	0	-	-	-	100
$PCL_{99.75}M_{0.25}$	0.25	-	-	-	99.75
$PCL_{99.3}M_{0.3}$	0.3	-	-	-	99.7
$PCL_{99.5}M_{0.5}$	0.5	-	-	-	99.5
$PCL_{99.25}M_{0.75}$	0.75	-	-	-	99.25
$PCL_{99}M_{1}$	1	-	-	-	99
$PCL_{98}M_{2}$	2	-	-	-	98
$PCL_{97}M_{3}$	3	-	-	-	97
$PCL_{95}M_{5}$	5	-	-	-	95
$PCL_{99.75}NH_{0.25}$	0.25	0.1	0.9	98.75	99.75[a]
$PCL_{99.5}NH_{0.5}$	0.5	0.2	1.8	97.5	99.5[a]
$PCL_{99.25}NH_{0.75}$	0.75	0.3	2.7	96.25	99.25[a]
$PCL_{99}NH_{1}$	1	0.4	3.7	95	99[a]
$PCL_{98}NH_{2}$	2	0.7	7.3	90	98[a]
$PCL_{97}NH_{3}$	3	1.0	11	85	97[a]

[a] In the nanohybrid, the total PCL is equal to the sum of g-PCL, "free" PCL and PCL of the matrix. In contrast, in the nanocomposites, the total PCL is equal to the PCL added in the blend.

ultramicrotome device at −25 °C equipped with a diamond knife. The ultrathin sections (∼100 nm) were placed on 300 mesh copper grip.

Differential Scanning Calorimetry

Calorimetric studies were carried out in a Perkin Elmer Diamond Differential Scanning Calorimeter (DSC) calibrated with indium and tin. Ultra-high purity nitrogen was used as a purge gas. Samples of approximately 5 mg each were encapsulated in aluminum pans and sealed. The crystalline thermal history was erased by heating the samples at 100 °C for 3 min. Cooling and subsequent heating scans were registered at 20 °C/min. The calorimetric analysis was performed only one time per sample per condition. The errors of the values reported corresponding to those expected on the basis of the DSC used, that is, −0.5 °C in temperatures and around 10% in enthalpies.

Self-Nucleation Tests (SN)

The self-nucleation (SN) test was performed according to procedures devised originally by Fillon et al.,[40,41] and recently reviewed by Michell et al.[42] and applied to nanocomposites incorporating CNT by Müller et al.[43–45] The complete procedure is as follows:

a. Hold at 100 °C for 3 min.
b. Creation of a "standard" thermal history by cooling at 20 °C/min to −10 °C.
c. Partial melting up to a temperature denoted T_s.
d. Thermal conditioning at T_s during 5 min.
e. DSC cooling scan at 20 °C/min from T_s to −10 °C.
f. Hold at −10 °C for 1 min.
g. DSC heating scan at 20 °C/min from −10 to 100 °C.

Isothermal Crystallization Experiments

The isothermal crystallization experiments were performed following the procedure given by Lorenzo et al.[46]

The minimum crystallization temperature was determined as follows:

a. The sample was heated to 100 °C and hold for 3 min to erase the thermal history.
b. Cooling at 60 °C/min down to a crystallization temperature, T_c.
c. Heating to 100 °C to check for the appearance of any melting signal.
d. Repeat steps (a) to (c) increasing the T_c until no signal in step (c) was observed.

The lowest temperature, at which no melting signal was detected, and this temperature were selected as the minimum crystallization temperature. After applying the above protocol, the neat PCL sample was isothermally crystallized in a temperature range from 35 to 43 °C. In the case of the nanocomposites, the T_c range was from 48 to 53 °C. The isothermal experimental crystallization time was about three times $\tau_{50\%}$ (i.e., the half-crystallization time).

Rheological Measurements

Sheet samples of neat materials and nanocomposites with 1 mm thickness were compression-molded with a Schwabenthan Polystat 200T hot press at a temperature of 100 °C and a pressure of 25–50 bars for 5 min and then cooled to room temperature. Melt rheological measurements were carried out using a stress-controlled Bohlin CVO rheometer from Malvern Instruments in both dynamic and static modes,

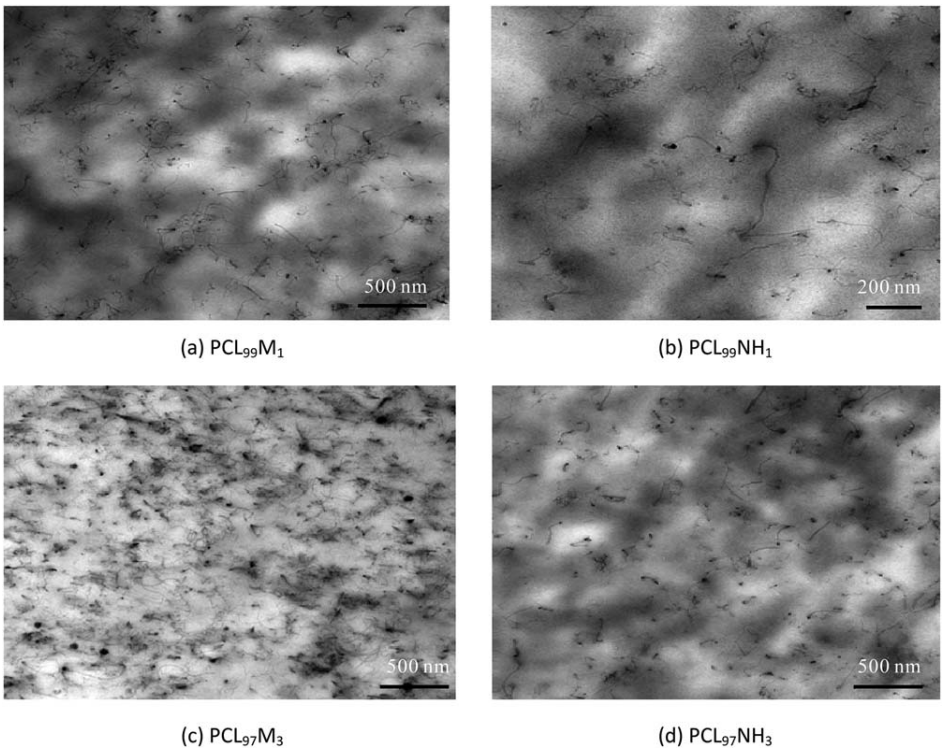

FIGURE 1 TEM Micrographs of (a,c) PCL_xM_y and (b,d) PCL_xNH_y with MWCNT Contents of 1 and 3% wt.

using parallel plates and cone-plate geometries. Dynamic oscillatory shear measurements were performed in the temperature range of 70–110 °C. The applied shear stress amplitudes correspond to shear strains of 0.05 or lower, which was proven to be in the linear viscoelastic regime for both the neat materials and the nanocomposites. The properties measured were the storage and the loss moduli, G' and G'', as well as the magnitude of the complex viscosity, $|\eta^*|$. Long creep experiments were also performed at a temperature of 70 °C. It was proven that the range of shear stress was within the linear regime (located below $\tau_0 = 100$ Pa in the materials studied). The time-dependent creep compliance, J_c, was also measured. Since these experiments take a long time, the thermal stability of the systems must be guaranteed. By comparing creep compliances and dynamic moduli that were measured in subsequent experiments and those that were determined directly after having installed the sample, the thermal stability of all the samples was demonstrated to be excellent at $T = 70$ °C, over periods of time of more than 24 h (100,000 s).

RESULTS AND DISCUSSION

Morphological Study

The samples were analyzed employing transmission electron microscopy (TEM). The dispersion of the nanotubes into the polymeric matrix is shown in Figure 1 for the samples indicated.

TEM observations were performed in nanocomposites containing 1 to 3 wt % CNTs. Also, two different types of blends were employed, those with the functionalized surface and other without functionalization, named PCLxNHy (nanohybrids) and PCLxMy (nanocomposites), respectively.

Figure 1 shows that the dispersion of MWCNT is similar for both PCL_xM_y [Fig. 1(a,c)] and PCL_xNH_y [Fig. 1(b,d)]. However, in the PCL_xM_y blend with 3 wt % of MWCNT, some agglomerates larger than in other compositions and also larger in comparison with PCL_xNH_y are found. The attachment of PCL chains on the MWCNTs avoids the agglomeration of MWCNTs resulting in an improvement of the dispersion.

Thermal Properties

Standard DSC Experiments

In Figure 2, the clear exothermic peaks during cooling are due to the crystallization of the PCL [Fig. 2(a)]. During subsequent heating scans, the sharp endothermic peaks represent the melting of the crystals formed during the previous step [Fig. 2(b)].

The crystallization temperature (T_c) is shifted to higher values as the number of carbon nanotubes increase, for both systems. This behavior has been already reported by several authors in the past, and it is associated with the nucleating ability of CNTs.[47–49] MWCNTs possess a large surface/volume ratio that provides an ideal substrate for the nucleation of polymer chains.[9,20–22,44,45,50–61]

Figure 3(a) shows the variation of the T_c with MWCNT content. The dramatic increase in T_c (16.2 °C) with only 1 wt % of MWCNT is an example of the nucleating capacity of the unmodified MWCNT. Similarly, the modified MWCNTs are able to increase T_c (15.1 °C) (see $PCL_{99}NH_1$).

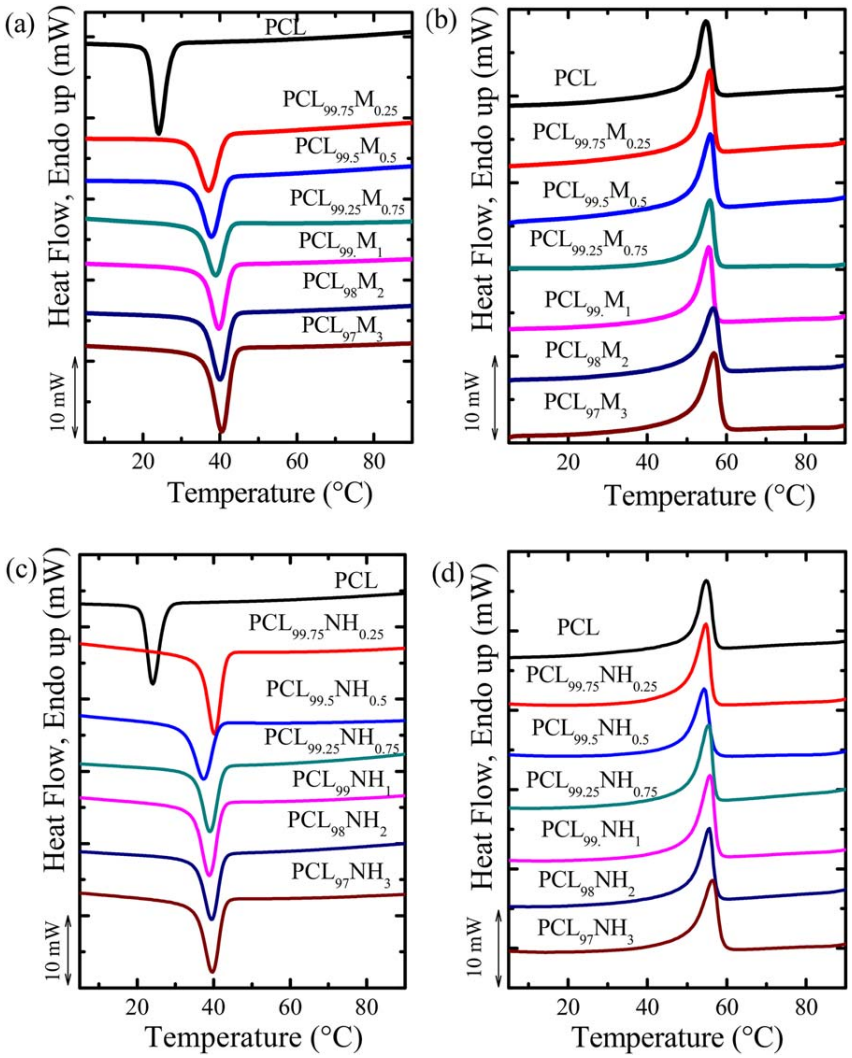

FIGURE 2 DSC cooling and heating scans at 20 °C/min for the indicated nanocomposites and nanohybrids. [Color figure can be viewed at wileyonlinelibrary.com]

In Figure 3(a), it is also observed that T_c is shifted to higher values as the unmodified MWCNT content is increased in the nanocomposites. The increase between 0.25 and 1 wt % of MWCNTs is higher than the one presented in a range of 1 to 3 wt %. This behavior is indicative of a saturation of the nucleating effect after 1 wt % loading with plain MWCNTs.

In contrast, for the modified MWCNTs, that is, in the nanohybrids, the trend is more complex because of the presence of PCL grafted chains onto the MWCNT surfaces. The grafted MWCNTs have a pearl-necklace-like structure (Supporting information Fig. S1) for some of the nanotubes with grafted PCL chains forming agglomerates on them. However, all the nanotubes are not covered by the grafted PCL chains. As a consequence, the applied chemical modification disentangles the CNTs, but grafted PCL chains do not cover all the surfaces of the nanotubes, thus leaving available MWCNT surface for PCL matrix nucleation. The drop in T_c values after 0.25 wt % and their recovery at higher loadings are attributed to a competition between the nucleation effect of MWCNT and the plasticization effect of both "free" PCL and PCL chains attached to the MWCNTs, which have a lower M_n values (i.e., 12,000 and 500–1000 g/mol, respectively) than the neat PCL matrix (i.e., 50,000 g/mol). As the MWCNT content increases in the hybrid materials, the number of low M_n PCL chains also increases (see Table 1). The low molecular weight PCL needs larger under-cooling than the high molecular weight to crystallize.[62] As a consequence, the shorter chains are molten during the crystallization process of the matrix, exhibiting a plasticization effect, as a result the undercooling needed by the PCL matrix should be larger as the amount of free PCL increases.

Müller et al. have studied supernucleation[11,43,45,61] effects for PEO-*g*-CNT, PCL-*g*-CNT and PE/CNT *in situ* polymerized nanocomposites. The term supernucleation refers to the nucleation by heterogeneities with efficiencies higher than the own polymer crystal fragments (see Self-nucleation and

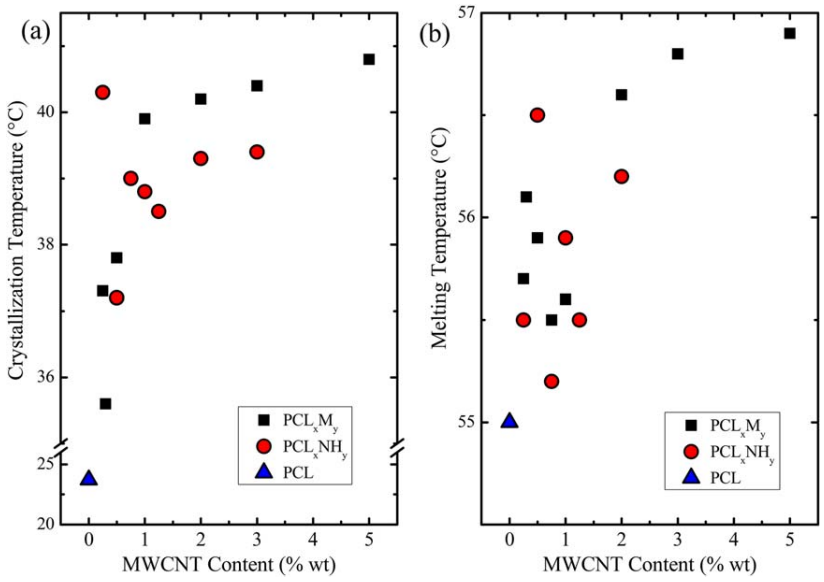

FIGURE 3 Influence of MWCNT content on (a) crystallization and (b) peak melting temperatures. [Color figure can be viewed at wileyonlinelibrary.com]

nucleation efficiency section below). A characteristic of this behavior is a large increase in T_c. Table 2 summarizes the results reported in the literature for PCL/CNT systems.

TABLE 2 Crystallization Temperature (T_c) Shift (Difference Between the T_c Value of Neat PCL and the T_c Value of the PCL with CNTs) for Different PCL/CNT Systems Reported in the Literature

System	MW or SWCNT (wt %)	Shift in T_c (°C)	Ref.
PCL/CNT	0.5	14	11
PCL/MWNT	5	2	9
PCL/MWNT	10	9	
	5	10	20
PCL-*g*-SWNT	5	14	22
PCL-*g*-fMWNT	2	4.5	41
PCL/MWCNT	0.25	13.6	This paper
	0.3	11.9	
	0.5	14.1	
	0.75	15.3	
	1	16.2	
	2	16.5	
	3	16.7	
PCL/PCL-*g*-MWNT	0.25	16.6	This paper
	0.5	13.5	
	0.75	15.3	
	1	15.1	
	2	15.6	
	3	15.7	

Not all reported works on PCL/CNT result in an increase in T_c. In fact, in some cases, an antinucleation effect has been reported. For instance, Jana et al.[63] reported a small decrease in T_c values for PCL-*g*-CNT nanocomposites prepared by a "grafting to" procedure. This contrasts with their report of a decrease in spherulitic size. The efficiency of a nucleating agent depends on, among other factors, the quality of the dispersion and distribution of the particles. According to the PLOM images showed by Jana et al., the quality of the distribution and dispersion was poor (as many agglomerates were visible), and it is possible that this originated the reduction in crystallization temperature.

Figure 3(b) as well as Table 3 show that the melting temperature (T_m) remains almost constant (i.e., it changes in between 55 and 57 °C) with the increase of the MWCNT content, as it is expected when a nucleating agent is employed. Although, it is worth mentioning that an increase of T_m has been reported in supernucleated PCL/CNT systems.[11,45]

Table 3 shows the variations of the crystallization degree for both systems. The calculations were performed employing an equilibrium melting enthalpy for a 100% crystalline PCL sample of 136 J/g.[64–66] In both cases, an increase in the degree of crystallinity is observed upon MWCNT addition. In general, the increase in MWCNT content results in an increase of X_c, although the trend is not monotonic. For example, the samples $PCL_{99.25}M_{0.75}$ and $PCL_{99.75}M_{0.25}$ exhibit apparent reductions in X_c, but the differences are small, and the error in enthalpy determination by DSC can be as large as 10–15%.

The increase of the crystallization degree with the increase in MWCNT content has also been reported by Trujillo et al.[11] for the PCL/MWCNT system. In contrast, some studies

TABLE 3 Crystallization and Melting Temperatures, Normalized Heat of Crystallization and Fusion, and Degree of Crystallinity (X_c) for the Nanocomposites

Sample	T_c (°C)	ΔH_c^n (J/g)	T_m (°C)	ΔH_m^n (J/g)	X_c (%)
PCL	23.7	51	55.0	54	40
$PCL_{99.75}M_{0.25}$	37.3	47	55.7	50	37
$PCL_{99.3}M_{0.3}$	35.6	56	56.1	58	42
$PCL_{99.5}M_{0.5}$	37.8	52	55.9	58	42
$PCL_{99.25}M_{0.75}$	39.0	47	55.5	52	38
$PCL_{99}M_1$	39.9	50	55.6	54	40
$PCL_{98}M_2$	40.2	54	56.6	63	46
$PCL_{97}M_3$	40.4	57	56.8	63	46
$PCL_{95}M_5$	40.8	55	56.9	58	43
$PCL_{99.75}NH_{0.25}$	40.3	65	55.5	69	51
$PCL_{99.5}NH_{0.5}$	37.2	57	56.5	63	46
$PCL_{99.25}NH_{0.75}$	39.0	60	55.2	64	47
$PCL_{99}NH_1$	38.8	68	55.9	76	55
$PCL_{98}NH_2$	39.3	56	55.5	63	45
$PCL_{97}NH_3$	39.4	64	56.2	71	51

reported a reduction in crystallinity for PCL/CNT and even in functionalized systems.[9,19–21,67] The authors explain this unusual behavior due to topological restrictions that constrain the chain diffusion during crystallization.[19] On several reports for nanocomposites of different polymeric matrices, the crystallinity can increase[52,55,60,68–71] or remains unchanged with CNT addition.[69] Once again, the interactions between the CNT and the polymer chain will determine the crystallization behavior of the system.

Self-Nucleation and Nucleation Efficiency

Self-nucleation experiments (SN) allow identifying the dependence of the melting temperature or self-nucleation (T_s) temperature on the subsequent crystallization process. According to Fillon et al.,[40,41] it is possible to identify three different domains. If T_s is high enough to melt all the crystals and crystalline memory, this T_s temperature belongs to *Domain I*. On the other hand lower T_s values will partially melt the crystals or leave some residual crystalline memory that can self-nucleate the material during cooling from T_s, in that case, the T_s temperature belongs to *Domain II*. Finally, even lower T_s temperatures can only partially melt the material, and unmolten crystals can anneal during the time the sample stays at T_s (usually 5 min), while the molten material can self-nucleate during cooling from T_s. These T_s temperatures belong to the *Domain III*.

The self-nucleation temperature that originates the largest amount of self-nuclei will be the lowest temperature belonging to *Domain II*. This temperature is called the ideal T_s ($T_{s,\ ideal}$). It is expected that T_c values after SN at $T_{s,\ ideal}$ are the highest temperature for the crystallization under non-isothermal conditions for a polymer. In fact, Fillon et al.[40,41] use such values as a reference to calculate the efficiency of a nucleating agent. For more information, a detailed overview can be found in reference 42 and its application to the nanocomposites case can be found in the following references 11,43–45,72, and 73.

An example of the experiment of self-seeding for the PCL employed in this work is shown in Figure 4. Figure 4(a) shows the cooling scans after SN at the indicated T_s, and Figure 4(b) shows the subsequent heating scans. After a careful observation of Figure 4(a) (the dashed line indicates the PCL crystallization temperature under standard conditions), it is possible to determine the change in the crystallization temperature without any change in the melting behavior. T_s values higher than 60 °C are high enough to produce a

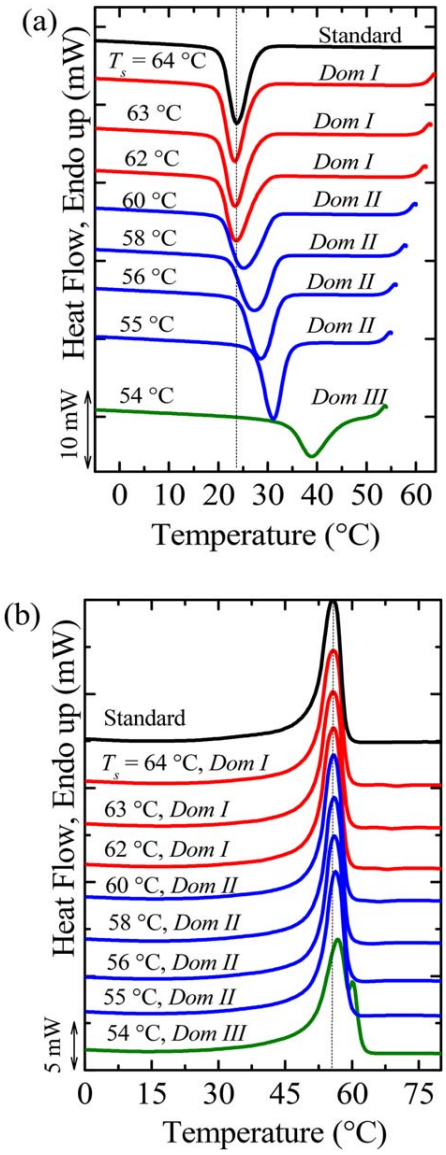

FIGURE 4 Self-nucleation behavior of neat PCL for selected self-nucleation temperatures (T_s). (a) DSC cooling scans from T_s and (b) DSC subsequent heating scans (see text). [Color figure can be viewed at wileyonlinelibrary.com]

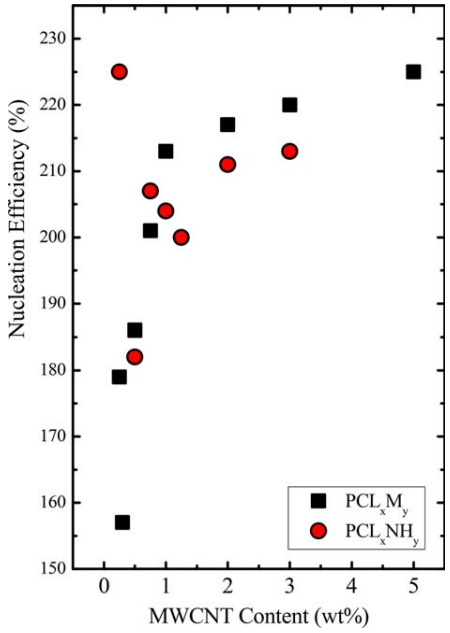

FIGURE 5 MWCNTs efficiencies as nucleating agents for PCL_xM_y and PCL_xNH_y nanocomposites. [Color figure can be viewed at wileyonlinelibrary.com]

complete melting process and a homogeneous melt. Lower or equal temperatures to 60 °C can produce self-nucleation in the melt (*Domain II* or self-nucleation Domain), in which T_c will increase with the decrease in T_s, but without changes in the melting scans (i.e., T_m should be the same for all the *Domain II*). Figure 4(b) shows a change in the melting process at 54 °C. At this point the melting endotherm shows a second peak at high temperatures indicating the presence of annealed crystals, which means that T_s values lower than 55 °C belong to *Domain III*. Since 54 °C belongs to *Domain III*, the ideal T_s should be 55 °C.

Employing the ideal T_s (55 °C), it is possible to find the maximum crystallization temperature ($T_{c,max}$) for the PCL employed here, that is, 31.3 °C.

The nucleation efficiency (*NE*) was calculated by Equation 1, developed by Fillon et al.[40] as follows:

$$NE = \frac{T_{c,NA} - T_{c,PCL}}{T_{c,\max} - T_{c,PCL}} x100 \quad (1)$$

where $T_{c,\ NA}$ is the peak crystallization temperature of the polymer with the nucleating agent, $T_{c,\ PCL}$ is the peak crystallization temperature of neat PCL after its crystalline history has been erased (23.7 °C) and $T_{c,max}$ is the maximum crystallization temperature after PCL has been self-nucleated at the ideal self-nucleation temperature (31.3 °C).

The results are shown in Figure 5. In all the cases, the nucleation efficiency is higher than 100%. This remarkable phenomenon is known as supernucleation since the crystallization temperature of the nanocomposites and nanohybrids are always higher than the crystallization temperature of the ideally self-nucleated polymer. The supernucleation has been reported in other systems such as *in situ* polymerized polyethylene on different carbon nanotubes[44,45] and PEO, and PCL covalently grafted on the surface of CNTs.[43,45] Trujillo et al.[11] reported for the first time the supernucleation in a simple melt mixed nanocomposite (PCL/CNT). This result indicated that the CNT supernucleation could be dominated by (a) the strong interaction between the polymer and the MWCNT and (b) the dispersion quality of the blend. In the present work, the supernucleation effect of the MWCNT is a result of an excellent dispersion of the MWCNT within the polymeric matrix, which can be enhanced when modified MWCNTs are employed. However, the improvement of the dispersion with the modification of MWCNT approach could lead to a decrease of its nucleation capacity, as a result of the agents introduced.

Isothermal Crystallization Experiments

The inverse of the half crystallization time ($1/\tau_{50\%}$) is related to the overall crystallization rate, which is plotted as a function of the crystallization temperature (T_c) in Figure 6. From Figure 6, it is possible to observe that the T_c range for isothermal crystallization of the PCL is much lower than for the nanocomposites. In the samples with MWCNTs, the supercooling needed for the development of isothermal crystallization is much lower than for neat PCL in view of the supernucleation effect that they cause on the PCL matrix.

A careful comparison of PCL_xM_y versus PCL_xNH_y samples reveals a complex behavior. At lower MWCNT content (0.25 wt %) the nanohybrids exhibit a higher crystallization rate than $PCL_{99.75}M_{0.25}$, but as the MWCNT content is increased (i.e., 0.25–1 wt %) the values of $1/\tau_{50\%}$ are closer, and remains almost the same until the MWCNT content reaches the value of 1 wt %, where the sample with pristine MWCNTs (i.e., nanocomposites) has a slightly higher crystallization rate than the nanohybrids.

This behavior in the MWCNT-*g*-PCL could be attributed to two competitive factors: (a) the nucleation ability of the MWCNT and (b) the diluent effect of the low molecular weight PCL chains grafted to the MWCNT. These chains could be acting as plasticizers reducing the crystallization kinetics. At lower MWCNT content, it is possible to obtain a favorable balance of these two factors, and the sample reaches the highest crystallization rate. In contrast, increases of MWCNTs content in the nanohybrids results in an increase in the number of low molecular weight PCL chains, which, in turns, increases the plasticizer effect.

A third factor may be possible, taking into account the works of Winey and coworkers.[74–78] They proposed that it is possible to modify the diffusion coefficient of a polymer chain when nanoparticles (NP) are present, or even in blends where the NP are grafted to polymer chains. They have reported that if the NPs are grafted to the polymer, the diffusion coefficient goes through a minimum as the NP concentration increases. Away from this minimum, high diffusion values are expected.

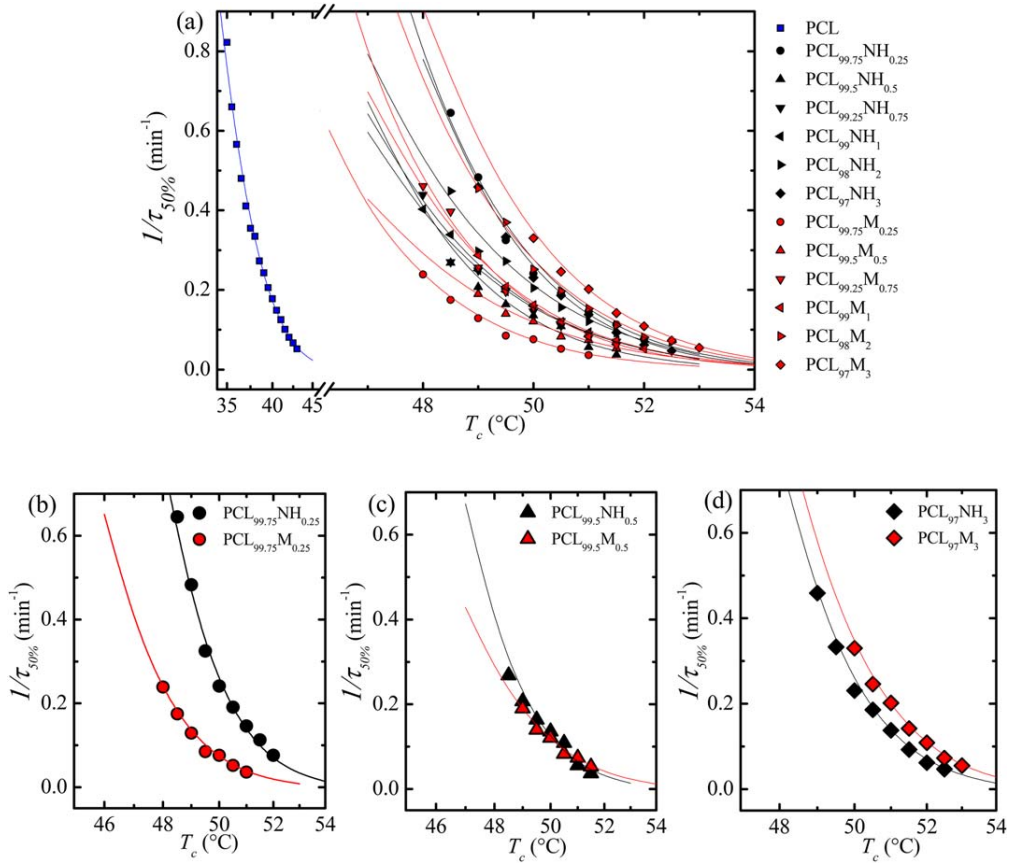

FIGURE 6 (a) Variation of $1/\tau_{50\%}$ (inverse of half-crystallization time) values as a function of the crystallization temperature for PCL_xM_y and PCL_xNHy samples. Solid lines indicate fittings to the Lauritzen and Hoffman theory. Selected pairs of samples (nanocomposites vs. nanohybrids) are compared for MWCNT contents of (b) 0.25, (c) 0.5 and (d) 3 wt %. [Color figure can be viewed at wileyonlinelibrary.com]

It could be possible that in the nanohybrids, a concentration of 0.25% MWCNT is within a region where maximum diffusion of polymer chains can occur next to the CNTs, and hence the overall crystallization can be accelerated.

The supercooling ($\Delta T = T_m^0 - T_c$) is proportional to the enthalpic driving force that a polymer needs to start the crystallization event, the reduction in ΔT is due to a reduction in the energy barrier as a consequence of the nucleating ability of the MWCNTs in both systems. Figure 7 shows the values of the crystallization temperature for which the blends reach a constant $1/\tau_{50\%}$ of 0.2 min^{-1} [Fig. 7(a)] and the $1/\tau_{50\%}$ values at a constant T_c of 52 °C [Fig. 7(b)], as a function of the MWCNT content. In Figure 7(a), it is possible to observe that T_c increases as MWCNT content increases. In other words, that ΔT is smaller when the amount of MWCNTs increases in the blend, suggesting that the presence of MWCNT (either in the PCL_xM_y or PCL_xNH_y) makes the overall crystallization (including both nucleation and growth) more favorable.

Figure 7(b) shows that the overall crystallization rate ($1/\tau_{50\%}$) increases with MWCNT content. This change can be attributed to the predominant increase in the nucleation rate. The overall crystallization rate has two components, the nucleation rate and the growth rate. As a consequence of the supernucleation found, a larger amount of nuclei are activated at higher temperature for both systems.

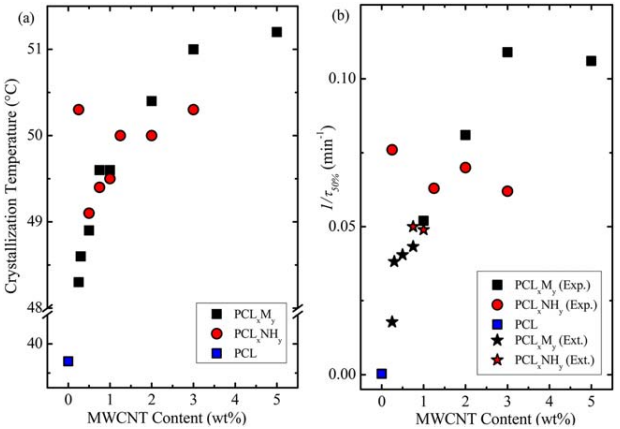

FIGURE 7 Influence of MWCNTs on (a) the crystallization temperature at $1/\tau_{50\%} = 0.2$ min^{-1} and on (b) the overall crystallization rate at $T_c = 52$ °C for the indicated blends. Different symbols are used for experimental (Exp.) and extrapolated (Ext.) data points. [Color figure can be viewed at wileyonlinelibrary.com]

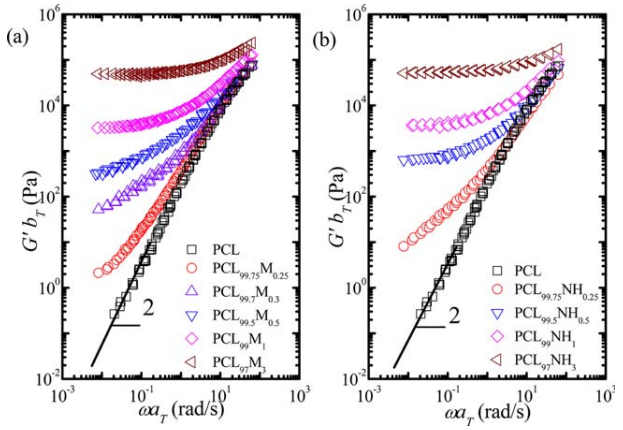

FIGURE 8 Reduced shear storage (G_{bT}) modulus versus reduced angular frequency (ω_{aT}) of the materials studied at T_R=70 °C. (a) PCL_xM_y and (b) PCL_xNH_y. [Color figure can be viewed at wileyonlinelibrary.com]

As a result, the rate of nucleation is increased, and the overall crystallization is also faster. The difference between the PCL_xM_y and PCL_xNH_y blends is small, suggesting that the modified MWCNTs have a similar activity than neat MWCNTs, except for the lowest content explored (i.e., 0.25 wt %).

The data obtained during the isothermal crystallization experiments were analyzed using the Avrami equation, which can be expressed as follows:[46,79]

$$1-V_c(t-t_0)=\exp\left(-K(t-t_0)^n\right) \quad (2)$$

where t is the experimental time, t_0 is the induction time, V_c is the relative volumetric transformed fraction, n is the Avrami index, and K is the overall crystallization rate constant. The procedure employed to perform the fittings to the Avrami equation was that given by Lorenzo et al.[46]

For all the samples studied, the fit was very good, even adjusting the data beyond the 50% of conversion. This behavior is not common but has been reported previously in some polyesters.[11,46,80] The Avrami indexes for PCL are between 2.7 and 3.2 (Supporting Information Table S1 and S2), these values are very close to 3 and correspond to instantaneously nucleated spherulites when they are observed by polarized light optical microscopy (not shown here). On the other hand, the introduction of highly active MWCNTs greatly increases the number of active nuclei, and, in consequence, a fully three-dimensional superstructure cannot be obtained for all the nanocomposites studied here, and small 2D lamellar aggregates are obtained instead (not shown here). The Avrami index was between 2.6 and 1.7 (Supporting Information Tables S1 and S2); however, the average was 2.3 and the most common value 2.1. These values correspond to a two-dimensional lamellar aggregates that resemble bottle brush morphologies or hybrid shish kebab structures observed in similar nanocomposites.[11,43,44,60] The K values are shown in the supplementary information (Supporting Information Tables S1 and S2). The values of $K^{1/n}$ display a similar tendency than $1/\tau_{50\%}$, since $K^{1/n}$ is also related to the overall crystallization kinetics.

Rheological Properties

The melt rheological data have been superposed using the time-temperature superposition principle to obtain master curves at a reference temperature, T_R.[81,82] Here we have selected a $T_R = 70$ °C. We have applied the method of Mavridis and Shroff,[82] to determine horizontal, a_T, and vertical, b_T, factors. The a_T and b_T values were extracted from tanδ versus ω and tanδ versus$|G^*|$ data, respectively. Both the a_T and b_T factors for the nanocomposites studied are similar to those of the unfilled polymer and obey an Arrhenius-type temperature dependence with horizontal activation energy around 40 kJ/mol (reported in the range 35.0–40.0 kJ/mol for PCL)[39,83] and vertical activation energies lower than 3.9 kJ/mol (< 1 kcal/mol).

The viscoelastic function storage moduli, G', for the neat polymer and the two families of nanocomposites are shown in Figure 8. The neat PCL behaves as a Newtonian liquid at low frequencies and shows the characteristic power law of the storage modulus, $G' \propto \omega^2$.[81] However, the terminal behavior disappears with the addition of MWCNTs either in PCL_xM_y or PCL_xNH_y. The low-frequency response for the samples display an increase of the values of G' and a decrease in the frequency dependence of G' (i.e., $G' \propto \omega^\beta$, with $\beta < 2$) within this region. This means that the long-time polymer dynamics in the terminal region is constrained by the presence of the MWCNTs.

As a result, the low-frequency complex viscosity, $|\eta^*|$, increases significantly in the presence of MWCNTs especially at high compositions, and the Newtonian plateau of the viscosity curve for PCL progressively vanishes, as it can be readily observed in Figure 9. This is associated with the formation of an MWCNT network, which leads to the transformation of the liquid-like

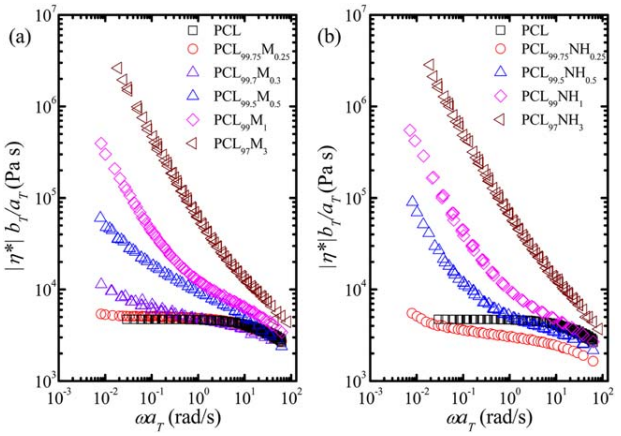

FIGURE 9 Reduced magnitude of the complex viscosity ($|\eta^*|\,b_T/a_T$) versus reduced angular frequency of the materials studied at T_R= 70 °C. (a) PCL_xM_y and (b) PCL_xNH_y. [Color figure can be viewed at wileyonlinelibrary.com]

polymer to a solid-like material showing a remarkable yield, even at very low MWCNT concentrations. The divergence of $|\eta^*|$ in the low-frequency zone (i.e., $|\eta^*| \propto \omega^{-\alpha}$, with $0 < \alpha < 1$) is clearly observed. Changes and improvements in the physical properties of polymers due to the addition of MWCNTs have been widely reported for polymeric nanocomposites with SWCNTs and MWCNTs, and it has been shown to depend on the MWCNT state of dispersion and aspect ratio, polymer-MWCNT interactions, but also on the molecular architecture of the polymeric matrix.[84–92]

In Figure 10, the exponents β and α (obtained by fitting in the lowest frequency decade experimentally available for G' and $|\eta^*|$), are plotted as a function of the MWCNT concentration. The value of β decreases monotonically from 2.0 to 0 with increasing MWCNT concentration and the values of α increase monotonically from 0 to 1.0, as it has been observed in well-dispersed PCL/SWCNT nanocomposites obtained by solution mixing,[33] which are included in Figure 10 for comparisons purposes. The behavior observed seems to be independent of the type of the MWCNTs in our case (i.e., PCL_xM_y and PCL_xNH_y).

The results in Figures 8–10 are associated with the formation of an MWCNT network, which leads to the transformation of the liquid-like polymer to a solid-like material, even at very low MWCNT concentrations. This behavior has been typically observed in yield stress (viscoplastic) materials. The yield stress is classically defined in the nonlinear viscoelastic range as the minimum shear stress that must be applied to a material (typically a multiphase system) to induce flow. The most common method to obtain the yield stress is to extrapolate the shear stress versus shear rate curve to zero shear rate, but there are other methods as stress relaxation, creep and recovery or shear stress ramp measurements. Dynamic oscillatory measurement is an alternative method for the determination of yield stress. Viscoplastic materials exhibit a low-frequency plateau in G', together with a characteristic power-law increase of $|\eta^*|$.

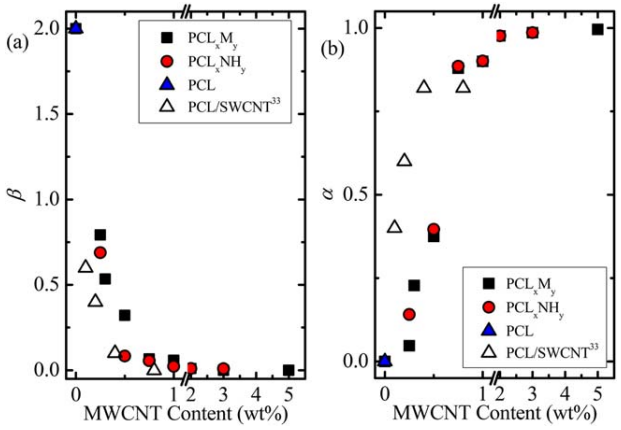

FIGURE 10 Power-law exponents of G' and $|\eta^*|$ obtained by fitting of the lowest frequencies. [Color figure can be viewed at wileyonlinelibrary.com]

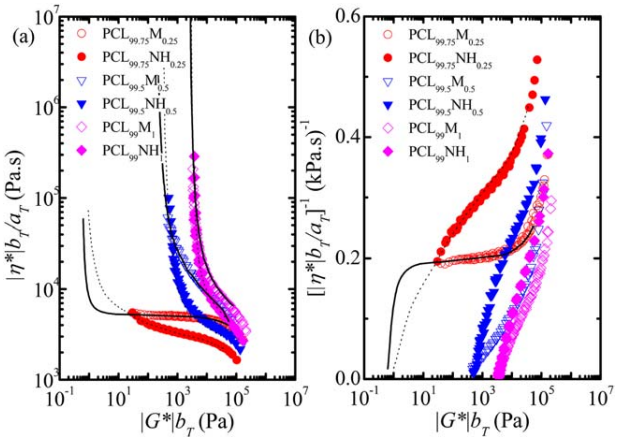

FIGURE 11 (a) Magnitude of the complex viscosity versus magnitude of the complex modulus of selected samples: (○) $PCL_{99.75}M_{0.25}$, (▽) $PCL_{99.5}M_{0.5}$, (◇) $PCL_{99}M_1$, (●) $PCL_{99.75}NH_{0.25}$, (▼) $PCL_{99.5}NH_{0.5}$, (◆) $PCL_{99}NH_1$. Lines represent the converted creep results to oscillatory data. (b) Extrapolation procedure using the creep results applied to obtain $|G^*|_0$ when $1/|\eta^*| \to 0$. [Color figure can be viewed at wileyonlinelibrary.com]

These trends have been suggested to be correlated to the yield stress. There is a vast amount of experimental results about multiphase systems that exhibit low-frequency plateaus in the G' and low-frequency power law in $|\eta^*|$, and also develop yield stress behavior in steady shear (see the recent monographic review about this matter by Malkin et al., [93]). There is a general agreement in that these behaviors at low frequencies are characteristic features of yielding fluids.

Obtaining the percolation threshold requires a full characterization of the yield behavior at low frequencies. It has been reported the possibility of estimate the value of the characteristic modulus of the network, $|G^*|_0$, from the $|G^*|$ versus $|\eta^*|$ plot.[33] In Figure 11, it is observed the typical plot of $|\eta^*|$ versus $|G^*|$ used for the study of materials that show yield behavior applied to our samples. In general, a well-defined yield is obtained in all the cases except for the samples with the lowest content in MWCNTs. Some authors have suggested a linear extrapolation of $|G^*|$ when $|\eta^*|$ tends to infinite (or the reciprocal tends to zero) to extract the typical modulus of the network.[33] In our case, this procedure works well for compositions higher than 0.25 wt %, as it can be observed in Figure 11(b). However, for the $PCL_{99.75}M_{0.25}$ and $PCL_{99.75}NH_{0.25}$ systems (those with the lowest MWCNT content), the application of this procedure would require very long extrapolations.

To further probe the existence and nature of this 'plateau', especially in these cases, we have performed long creep measurements at $T = 70$ °C. The shear compliance, J_c, obtained from these measurements is shown in Figure 12 for selected samples. The results for J_c are within the linear viscoelastic region, as it is guaranteed by the identical trend obtained for each material irrespective of the shear stress applied in the range $\tau_0 = 6.25$–100 Pa.

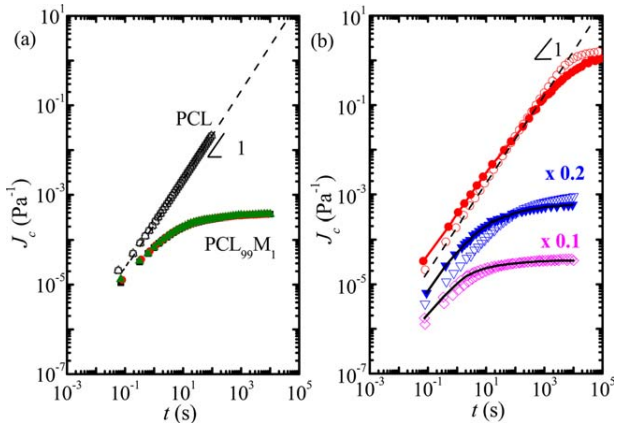

FIGURE 12 (a) Shear creep compliance, J_c, as a function of creep time for selected materials at $T = 70$ °C. Applied shear stress, τ_0: (○) 6.25 Pa, (□) 12.5 Pa, and (△) 25 Pa for PCL and (■) 50 Pa, (●) 75 Pa, and (▲) 100 Pa for $PCL_{99}M_1$. Dotted lines indicate the extrapolated slope of the flow region for PCL. (b) Shear creep compliance, J_c, as a function of creep time at $T = 70$ °C for pure PCL (dashed line); MWCNT samples: (○) $PCL_{99.75}M_{0.25}$, (▽) $PCL_{99.5}M_{0.5}$, (◇) $PCL_{99}M_1$; and the NH samples (●) $PCL_{99.75}NH_{0.25}$, (▼) $PCL_{99.5}NH_{0.5}$, (◆) $PCL_{99}NH_1$. The curves of the samples with 0.5 and 1 wt % MWCNT content in (b) have been vertically shifted for a better visualization, as indicated in the graph. [Color figure can be viewed at wileyonlinelibrary.com]

In Figure 12(a), the results obtained for PCL and $PCL_{99}M_1$ are shown as examples. The creep mode allows one to work in the terminal region providing application of low enough values of shear stress for long creep times. Typically, in polymeric materials, it is possible to obtain the value of Newtonian viscosity, η_0, as$\eta_0 = \lim_{tJJ}$ t/J(t). This is the case of the neat PCL sample, which shows the typical behavior of a Newtonian polymer in the whole time window explored, with $J_c \propto t^1$. Lower values of J_c are observed as the MWCNT content in the sample increases [Fig. 12(b)]. The terminal behavior, however, is not reached in any of the nanocomposites within the time window explored. The addition of the MWCNTs becomes evident by a general decrease of J_c over the whole ranges of time for the samples, either in PCL_xM_y or PCL_xNH_y samples. The most interesting result is that in all cases, including the samples with the lowest content in MWCNT, a constant "plateau" in compliance is reached at long times, indicating the expected solid-like behavior of percolated networks. The equilibrium values of J_c at long times are quite similar in both families at a given content of MWCNTs, as it is shown in Figure 12(b).

TABLE 4 Solid-Like Yield Complex Modulus for the Materials Under Study at $T = 70$ °C

PCL_xM_y	$\|G^*\|_0$ (Pa)	PCL_xNH_y	$\|G^*\|_0$ (Pa)
$PCL_{99.75}M_{0.25}$	0.63	$PCL_{99.75}NH_{0.25}$	1.0
$PCL_{99.3}M_{0.3}$	15	–	–
$PCL_{99.5}M_{0.5}$	220	$PCL_{99.5}NH_{0.5}$	340
$PCL_{99.25}M_{0.75}$	1,640	$PCL_{99.25}NH_{0.75}$	1,810
$PCL_{99}M_1$	2,710	$PCL_{99}NH_1$	2,960
$PCL_{98}M_2$	18,000	$PCL_{98}NH_2$	20,000
$PCL_{97}M_3$	52,500	$PCL_{97}NH_3$	55,000
$PCL_{95}M_5$	142,900	–	

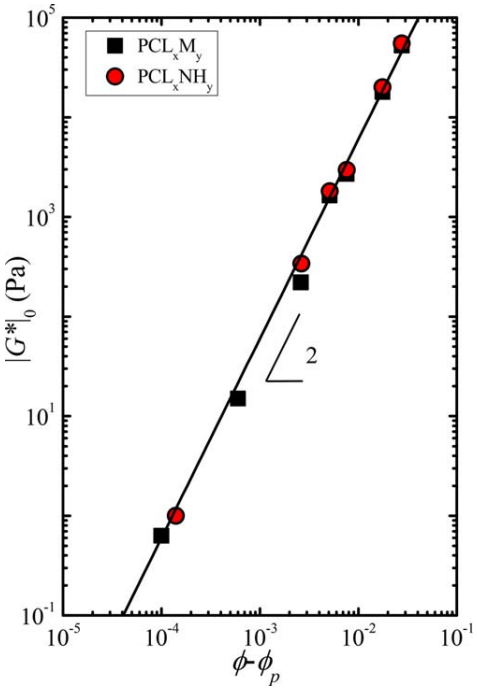

FIGURE 13 Linearization of the compositional dependence of the yield "plateau" modulus for the systems under study. The line is the best fit to eq 3. [Color figure can be viewed at wileyonlinelibrary.com]

The values of J_c in Figure 12 have been converted to $|G^*|$ and $|\eta^*|$, following the procedures described elsewhere.[94–96] These procedures have been reported to work very well in polymeric nanocomposites, provided that the linear viscoelastic region is guaranteed.[91] The results obtained from the experiments can then be compared in a broad range of angular frequencies, as it is observed in Figure 11(b) for the $|G^*|$ versus $|\eta^*|$ plot. The strong effect of the MWCNTs can be seen, even for the lowest MWCNT compositions. From this plot, the characteristic values of $|G^*|_0$ for the MWCNT network have been obtained. The values are listed in Table 4.

The application of the percolation theory to the results obtained for $|G^*|_0$ from the combination of oscillatory and creep experiments as a function of the MWCNT content is shown in Figure 13. The determination of the critical concentration, ϕ_p, is made by fitting the data to the following scaling law:

$$|G^*|_0(\phi) = |G^*|_0(\phi - \phi_p)^t \quad (3)$$

The critical concentration was found to be quite similar in both families within the experimental uncertainty, 0.240%

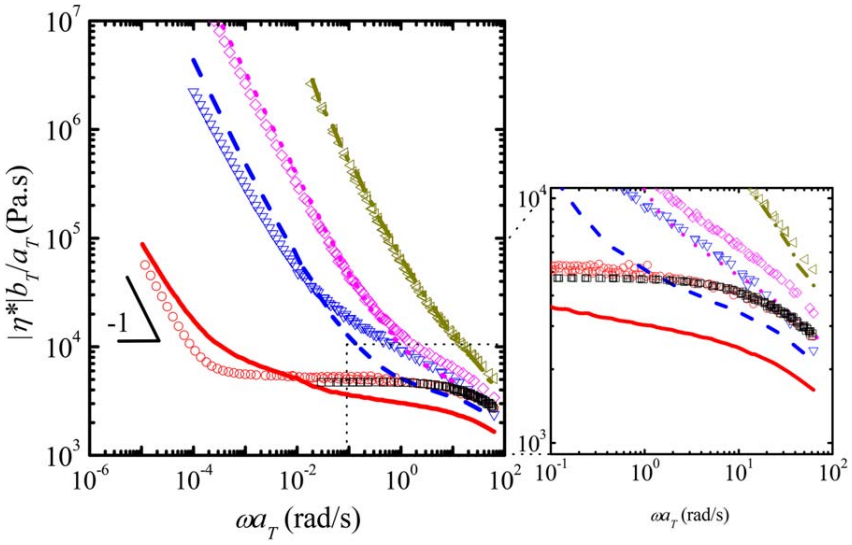

FIGURE 14 Reduced magnitude of the complex viscosity, obtained from oscillatory and transformed creep experiments, versus reduced angular frequency of selected samples: (□) PCL, (○) $PCL_{99.75}M_{0.25}$, (▽) $PCL_{99.5}M_{0.5}$, (◇) $PCL_{99}M_1$, (◁) $PCL_{97}M_3$, (solid line) $PCL_{99.75}NH_{0.25}$, (dashed line) $PCL_{99.5}NH_{0.5}$, (dotted line) $PCL_{99}NH_1$, (dash-dotted line) $PCL_{97}NH_3$. [Color figure can be viewed at wileyonlinelibrary.com]

and 0.236 wt % for PCL_xM_y and PCL_xNH_y families, respectively. The volume fraction, ϕ_p, is around 1.5×10^{-3}, assuming a density $\rho_{PCL(melt)}=1.06$ g/cm^3 at $T=$ 70 °C[97] and $\rho_{MWCNT}=1.74$ g/cm^3.[98] The critical exponent in Equation 3 is $t=2.00$, which is agreement with the universal value expected in the case of a 3D percolated network.[99,100] The percolation threshold obtained is one order of magnitude lower than those obtained in previous determinations on PCL/CNT (2–3 wt %),[24,35] and slightly lower than that obtained recently by Chin et al. (0.3 wt %),[34] in samples prepared by melt mixing. These last results together with those obtained in our systems are well within the range observed in PCL/CNT prepared by solvent dispersion (0.07–0.7 wt %),[25,33] suggesting a good dispersion of the MWCNTs in the polymer matrix for our samples. It should be noted that the geometrical threshold is also dependent upon the dimensions and effective anisotropy of the dispersed objects, and so we have to take into account the differences when comparisons are made.

A closer inspection of the results obtained for $|G^*|_0$ at given compositions suggests a slightly better dispersion for the PCL_xNH_y family (see Table 4). This is also clear in the complex viscosity plot shown in Figure 14. The figure includes a combination of oscillatory and creep results for selected samples at $T=70$ °C. It is observed that both families reach in the low-frequency region the expected yield behavior ($|\eta^*|\propto\omega^{-1}$). Additionally, PCL_xNH_y samples reach higher values of $|\eta^*|$ than the analogous PCL_xM_y. These results suggest that: (i) the MWCNT network dominates the dynamics of the systems within low-frequency (long time) region in both families, restricting polymer chains terminal relaxation and (ii) the MWCNT network in the PCL_xNH_y family restricts more efficiently this relaxation than in PCL_xM_y samples, at least up to MWCNT content of 1 wt %.

More interesting differences between PCL_xM_y and PCL_xNH_y families can be observed for $|\eta^*|$ in the high-frequency region. An enlargement of this specific region is observed in the right panel of Figure 14. It is remarkable that for those samples with the lowest NH content, $|\eta^*|$ diverges from that obtained for the neat PCL and PCL_xM_y family, decreasing in magnitude up to a 50% (see the solid lines in Fig. 14). The equivalent is observed for creep compliance in Figure 12(b) at short times, with a clear increase in J_c values with respect to that observed in neat PCL.

The decreased viscosity and increased compliance is a result of the low molecular weight free and grafted PCL chains in PCL_xNH_y samples, as a consequence of the process of functionalization of the MWCNTs. At high frequencies, the mechanical solicitation acts on a small size scale, being less sensitive to the MWCNT network, as it is demonstrated by the small changes observed for the PCL_xM_y family with respect to the neat PCL. For example, in this zone, the $PCL_{99.75}M_{0.25}$ is virtually identical to neat PCL. However, this is not the case for the PCL_xNH_y, for which the effect of the low molecular weight species (either grafted or "free') have a measurable effect. The influence of these low molecular weight species vanishes as the NH content increases. In fact, the plasticization effect disappears for compositions higher than 1 wt %, within the frequency range experimentally available, as it is observed in Figure 14. This is most probably due to a shift of the plasticization effect at higher frequencies as NH content increases. It should be noted that in the rheological analysis two competing mechanisms push in opposite directions as NH content increases: (i) an increase in the amount of low-M_w PCL component (decrease the magnitude of the rheological properties), and (ii) a decrease of the mesh size of the MWCNT network (increase the magnitude of the rheological properties). For the highest NH

content, the plasticization range may shift outside the experimentally accessible area due to the extremely low mesh size of the MWCNT network.

The results observed for the PCL_xNH_y family may have important implications in process operations, such as extrusion. It should be recalled here that PCL has been reported to show significant and undesirable extrudate distortions during this process.[101] The results shown here are promising, as they anticipate a better performance and processability of the PCL_xNH_y samples in extrusion processes, preventing or delaying extrudate distortions, and also conferring a better dimensional stability, as it has been observed in polyolefins such as polypropylene and polyethyene.[102,103]

CONCLUSIONS

The comparative study of the crystallization process of the PCL_xM_y and PCL_xNHy systems shows common behaviors such as the supernucleating action of the carbon nanotubes in the crystallization process and the increase in the rate of crystallization with the content of nanotubes as compared to PCL homopolymer. A novel aspect of this study is the significant influence of the molecular weight of the PCL chains synthesized during the functionalization of the nanotubes, whether they are free or grafted, in the overall crystallization kinetics and therefore in the solidification process of products. The nucleating action of the nanotubes and the plasticizing effect of the low molecular weight PCL chains synthesized during the functionalization have opposite effects on the crystallization kinetics of the nanohybrids. The prevalence of one effect with respect to the other exhibits an interesting dependence on the composition. This competition illustrates the greater complexity of nanohybrid systems with respect to nanocomposites. Nanohybrids with 1 wt % or less MWCNTs exhibit faster crystallization rates than nanocomposites. In contrast, nanohybrid with more than 1 wt % MWCNT exhibit lower crystallization rates than nanocomposites, as a consequence of the plasticization action of low molecular weight PCL chains. The control of the molecular weight of the grafted and "free" chains in nanohybrid systems offers a novel way to tailor the behavior of these systems.

Rheological properties confirm solid-like behavior in the melt for both PCL_xM_y and PCL_xNH_y samples from MWCNT content as low as 0.25 wt %. The results indicate an effective dispersion of the MWCNT in both families, and a percolation threshold of around 0.23–0.24 wt %, which is one order of magnitude lower than that found in other melt-mixed PCL nanocomposites. The application of the percolation theory to the rheological data confirms a 3D percolated network in the melt, with an exponent $t = 2.00$. Additionally, from this study, an improved performance and processability of the PCL_xNH_y samples can be foreseen, as decreased values of viscosity (up to a 50%) have been determined in the compositional range 0.25–1 wt % of nanohybrids. This result is likely due to the low molecular weight MWCNT-grafted and "free" PCL present in PCL_xNH_y samples, which compete with the MWCNTs network for these compositions.

ACKNOWLEDGMENTS

The authors acknowledge funding support from: the Spanish Ministerio de Economía y Competitividad (MINECO) for the Project: MAT2012-36341-FEDER, Decanato de Investigación y Desarrollo Universidad Simón Bolívar DID G02. The POLYMAT/UPV/EHU team acknowledges funding from the following projects: "UPV/EHU Infrastructure: INF 14/38"; "Mineco/FEDER: SINF 130I001726XV1/Ref.: UNPV13–4E10–1726," and "MinecoMAT2014–53437-C2-P." R. A. Pérez-Camargo gratefully acknowledges the award of a PhD fellowship by POLYMAT Basque Center for Macromolecular Design and Engineering.

AUTHOR CONTRIBUTIONS

J. F. Vega supervised the rheological characterization, its analysis and contributed writing the rheological part of the manuscript.

J. Fernández-Alcázar performed the rheology experiments.

J. V. López performed the DSC experiments.

R. M. Michell planned and supervised the thermal characterization of the materials and help in the interpretation of the results and in writing part of the paper.

M. L. Arnal contributed to the analysis of the DSC data and their interpretation.

R. A. Pérez-Camargo performed the morphological characterization (TEM) and contributed to the analysis of the results.

B. Ruelle synthesized the nanohybrid samples and prepared the blends PCL/NTC and PCL/nanohybrids.

P. Dubois designed the synthesis of the nanohybrids and supervised the preparation of the nanocomposites.

J. Martínez-Salazar contributed to the design and interpretation of the rheological experiments.

A. J. Müller planned and coordinated this collaborative work. He also contributed to the interpretation of the results and to the writing of the paper.

REFERENCES AND NOTES

1 P. M. Ajayan, In *Handbook of Nanostructured Materials and Nanotechnology*; Academic Press: Burlington, **2000**, p 375–406.

2 C. Wang, Z.-X. Guo, S. Fu, W. Wu, D. Zhu, *Prog. Polym. Sci.* **2004**, *29*, 1079–1141.

3 M. Moniruzzaman, K. I. Winey, *Macromolecules* **2006**, *39*, 5194–5205.

4 A. P. Kumar, D. Depan, N. Singh Tomer, R. P. Singh, *Prog. Polym. Sci.* **2009**, *34*, 479–515.

5 B. P. Grady, *J. Polym. Sci. Part B: Polym. Phys.* **2012**, *50*, 591–623.

6 S. Sathyanarayana, C. Hübner, In *Structural Nanocomposites: Perspectives for Future Applications;* J. Njuguna, Ed.; Springer Berlin Heidelberg: Berlin, Heidelberg, **2013**; Chapter 2, p 19–60.

7 M. Castro, J. Lu, S. Bruzaud, B. Kumar, J.-F. Feller, *Carbon* **2009**, *47*, 1930–1942.

8 K. Saeed, S.-Y. Park, H.-J. Lee, J.-B. Baek, W.-S. Huh, *Polymer* **2006**, *47*, 8019–8025.

9 M. D. Sanchez-Garcia, J. M. Lagaron, S. V. Hoa, *Compos. Sci. Technol.* **2010**, *70*, 1095–1105.

10 I. Armentano, M. Dottori, E. Fortunati, S. Mattioli, J. M. Kenny, *Polym. Degrad. Stab.* **2010**, *95*, 2126–2146.

11 M. Trujillo, M. L. Arnal, A. J. Müller, M. A. Mujica, C. Urbina de Navarro, B. Ruelle, P. Dubois, *Polymer* **2012**, *53*, 832–841.

12 L. Pan, X. Pei, R. He, Q. Wan, J. Wang, *Colloids Surf. B Biointerfaces* **2012**, *93*, 226–234.

13 K. D. McKeon-Fischer, D. H. Flagg, J. W. Freeman, *J. Biomed. Mater. Res. Part A* **2011**, *99A*, 493–499.

14 C. W. Tan, K. H. Tan, Y. T. Ong, A. R. Mohamed, S. H. S. Zein, S. H. Tan, *Environ. Chem. Lett.* **2012**, *10*, 265–273.

15 E. Heister, E. W. Brunner, G. R. Dieckmann, I. Jurewicz, A. B. Dalton, *ACS Appl. Mater. Interfaces* **2013**, *5*, 1870–1891.

16 H. L. Zeng, C. Gao, D. Y. Yan, *Adv. Funct. Mater.* **2006**, *16*, 812–818.

17 S. C. Tjong, *Mater. Sci. Eng.: R. Rep.* **2006**, *53*, 73–197.

18 H.-S. Kim, Y. S. Chae, J. H. Choi, J.-S. Yoon, H. Jin, *J. Adv. Compos. Mater.* **2008**, *17*, 157–166.

19 J.-T. Yeh, M.-C. Yang, C.-J. Wu, C.-S. Wu, *J. Appl. Polym. Sci.* **2009**, *112*, 660–668.

20 T.-M. Wu, E.-C. Chen, *J. Polym. Sci. Part B: Polym. Phys.* **2006**, *44*, 598–606.

21 T.-M. Wu, E.-C. Chen, *Polym. Eng. Sci.* **2006**, *46*, 1309–1317.

22 C. A. Mitchell, R. Krishnamoorti, *Polymer* **2005**, *46*, 8796–8804.

23 A. Bello, E. Laredo, J. R. Marval, M. Grimau, M. L. Arnal, A. J. Müller, B. Ruelle, P. Dubois, *Macromolecules* **2011**, *44*, 2819–2828.

24 D. Wu, L. Wu, Y. Sun, M. Zhang, *J. Polym. Sci. Part B: Polym. Phys.* **2007**, *45*, 3137–3147.

25 J.-M. Thomassin, X. Lou, C. Pagnoulle, A. Saib, L. Bednarz, I. Huynen, R. Jérôme, C. Detrembleur, *J. Phys. Chem. C* **2007**, *111*, 11186–11192.

26 A. Einstein, *Ann. Phys.* **1906**, *324*, 371–381.

27 T. Chatterjee, R. Krishnamoorti, *Soft Matter* **2013**, *9*, 9515–9529.

28 G. Filippone, M. Salzano de Luna, *Macromolecules* **2012**, *45*, 8853–8860.

29 F. J. Galindo-Rosales, P. Moldenaers, J. Vermant, *Macromol. Mater. Eng.* **2011**, *296*, 331–340.

30 L. A. Hough, M. F. Islam, P. A. Janmey, A. G. Yodh, *Phys. Rev. Lett.* **2004**, *93*, 168102.

31 D. W. Litchfield, D. G. Baird, *Rheol. Rev.* **2006**, *2006*, 60.

32 Q. Zhang, F. Fang, X. Zhao, Y. Li, M. Zhu, D. Chen, *J. Phys. Chem. B* **2008**, *112*, 12606–12611.

33 C. A. Mitchell, R. Krishnamoorti, *Macromolecules* **2007**, *40*, 1538–1545.

34 S. J. Chin, S. Vempati, P. Dawson, M. Knite, A. Linarts, K. Ozols, T. McNally, *Polymer* **2015**, *58*, 209–221.

35 K. Saeed, S.-Y. Park, *J. Appl. Polym. Sci.* **2007**, *104*, 1957–1963.

36 B. Ruelle, S. Peeterbroeck, T. Godfroid, C. Bittencourt, M. Hecq, R. Snyders, P. Dubois, *Polymers* **2012**, *4*, 296.

37 B. Ruelle, S. Peeterbroeck, C. Bittencourt, G. Gorrasi, G. Patimo, M. Hecq, R. Snyders, S. D. Pasquale, P. Dubois, *React. Funct. Polym.* **2012**, *72*, 383–392.

38 H. Kong, C. Gao, D. Yan, *Macromolecules* **2004**, *37*, 4022–4030.

39 J. Gimenez, P. Cassagnau, A. Michel, *J. Rheol.* **2000**, *44*, 527–547.

40 B. Fillon, J. C. Wittmann, B. Lotz, A. Thierry, *J. Polym. Sci. Part B: Polym. Phys.* **1993**, *31*, 1383–1393.

41 B. Fillon, A. Thierry, J. C. Wittmann, B. Lotz, *J. Polym. Sci. Part B: Polym. Phys.* **1993**, *31*, 1407–1424.

42 R. M. Michell, A. Mugica, M. Zubitur, A. J. Müller, In *Polymer Crystallization I: From Chain Microstructure to Processing*. Springer: Berlin, Heidelberg, **2015**; p 1–42.

43 D. Priftis, G. Sakellariou, N. Hadjichristidis, E. K. Penott, A. T. Lorenzo, A. J. Müller, *J. Polym. Sci. Part A: Polym. Chem.* **2009**, *47*, 4379–4390.

44 M. Trujillo, M. L. Arnal, A. J. Müller, E. Laredo, S. Bredeau, D. Bonduel, P. Dubois, *Macromolecules* **2007**, *40*, 6268–6276.

45 A. J. Müller, M. L. Arnal, M. Trujillo, A. T. Lorenzo, *Eur. Polym. J.* **2011**, *47*, 614–629.

46 A. T. Lorenzo, M. L. Arnal, J. Albuerne, A. Müller, *J. Polym. Test.* **2007**, *26*, 222–231.

47 L. Mandelkern, *Crystallization of Polymers: Volume 1, Equilibrium Concepts*; Cambridge University Press: New York, **2002**.

48 L. Mandelkern, *Crystallization of Polymers: Volume 2, Kinetics and Mechanisms*; Cambridge University Press: New York, **2004**.

49 G. Strobl, In *Progress in Understanding of Polymer Crystallization;* Reiter, G.; Strobl, G., Eds.; Springer Berlin Heidelberg: Berlin, **2007**, p 481–502.

50 R. Andrews, M. C. Weisenberger, *Curr. Opin. Solid State Mater. Sci.* **2004**, *8*, 31–37.

51 R. Haggenmueller, J. E. Fischer, K. I. Winey, *Macromolecules* **2006**, *39*, 2964–2971.

52 B. P. Grady, F. Pompeo, R. L. Shambaugh, D. E. Resasco, *J. Phys. Chem. B* **2002**, *106*, 5852–5858.

53 A. R. Bhattacharyya, T. V. Sreekumar, T. Liu, S. Kumar, L. M. Ericson, R. H. Hauge, R. E. Smalley, *Polymer* **2003**, *44*, 2373–2377.

54 O. Probst, E. M. Moore, D. E. Resasco, B. P. Grady, *Polymer* **2004**, *45*, 4437–4443.

55 M. L. Minus, H. G. Chae, S. Kumar, *Polymer* **2006**, *47*, 3705–3710.

56 K. P. Ryan, S. M. Lipson, A. Drury, M. Cadek, M. Ruether, S. M. O'Flaherty, V. Barron, B. McCarthy, H. J. Byrne, W. J. Blau, J. N. Coleman, *Chem. Phys. Lett.* **2004**, *391*, 329–333.

57 S. P. Bao, S. C. Tjong, *Mater. Sci. Eng. A* **2008**, *485*, 508–516.

58 K. Anoop Anand, U. S. Agarwal, R. Joseph, *Polymer* **2006**, *47*, 3976–3980.

59 Y. Gao, Y. Wang, J. Shi, H. Bai, B. Song, *Polym. Test.* **2008**, *27*, 179–188.

60 G. Xu, L. Du, H. Wang, R. Xia, X. Meng, Q. Zhu, *Polym. Int.* **2008**, *57*, 1052–1066.

61 M. Trujillo, M. L. Arnal, A. J. Müller, S. Bredeau, D. Bonduel, P. Dubois, I. W. Hamley, V. Castelletto, *Macromolecules* **2008**, *41*, 2087–2095.

62 M. J. Jenkins, K. L. Harrison, *Polym. Adv. Technol.* **2006**, *17*, 474–478.

63 R. N. Jana, J. W. Cho, *Compos. Part A: Appl. Sci. Manufact.* **2010**, *41*, 1524–1530.

64 P. J. Phillips, G. J. Rensch, K. D. Taylor, *J. Polym. Sci. Part B: Polym. Phys.* **1987**, *25*, 1725–1740.

65 Q. Guo, G. Groeninckx, *Polymer* **2001**, *42*, 8647–8655.

66 S.-W. Kuo, S.-C. Chan, F.-C. Chang, *J. Polym. Sci. Part B: Polym. Phys.* **2004**, *42*, 117–128.

67 F. Buffa, H. Hu, D. E. Resasco, *Macromolecules* **2005**, *38*, 8258–8263.

68 H.-S. Xu, X. J. Dai, P. R. Lamb, Z.-M. Li, *J. Polym. Sci. Part B: Polym. Phys.* **2009**, *47*, 2341–2352.

69 Y. Li, Y. Wang, L. Liu, L. Han, F. Xiang, Z. Zhou, *J. Polym. Sci. Part B: Polym. Phys.* **2009**, *47*, 326–339.

70 A. M. Díez-Pascual, M. Naffakh, M. A. Gómez, C. Marco, G. Ellis, M. T. Martínez, A. Ansón, J. M. González-Domínguez, Y. Martínez-Rubi, B. Simard, *Carbon* **2009**, *47*, 3079–3090.

71 J. Y. Kim, S. I. Han, D. K. Kim, S. H. Kim, *Compos. Part A: Appl. Sci. Manufact.* **2009**, *40*, 45–53.

72 R. A. Pérez, J. V. López, J. N. Hoskins, B. Zhang, S. M. Grayson, M. T. Casas, J. Puiggalí, A. J. Müller, *Macromolecules* **2014**, *47*, 3553–3566.

73 R. A. Pérez-Camargo, G. Saenz, S. Laurichesse, M. T. Casas, J. Puiggalí, L. Avérous, A. J. Müller, *J. Polym. Sci. Part B: Polym. Phys.* **2015**, *53*, 1736–1750.

74 C.-C. Lin, K. Ohno, N. Clarke, K. I. Winey, R. J. Composto, *Macromolecules* **2014**, *47*, 5357–5364.

75 A. Karatrantos, R. J. Composto, K. I. Winey, M. Kröger, N. Clarke, *Macromolecules* **2012**, *45*, 7274–7281.

76 M. Mu, N. Clarke, R. J. Composto, K. I. Winey, *Macromolecules* **2009**, *42*, 7091–7097.

77 M. Mu, R. J. Composto, N. Clarke, K. I. Winey, *Macromolecules* **2009**, *42*, 8365–8369.

78 J. Choi, N. Clarke, K. I. Winey, R. J. Composto, *ACS Macro Lett.* **2014**, *3*, 886–891.

79 M. Avrami, *J Chem. Phys.* **1939**, *7*, 1103–1112.

80 R. M. Michell, A. J. Müller, M. Spasova, P. Dubois, S. Burattini, B. W. Greenland, I. W. Hamley, D. Hermida-Merino, N. Cheval, A. Fahmi, *J. Polym. Sci. Part B: Polym. Phys.* **2011**, *49*, 1397–1409.

81 J. D. Ferry, *Viscoelastic Properties of Polymers*, 3rd Ed.; Willey: New York, **1980**.

82 H. Mavridis, R. N. Shroff, *Polym. Eng. Sci.* **1992**, *32*, 1778–1791.

83 D. H. S. Ramkumar, M. Bhattacharya, *Polym. Eng. Sci.* **1998**, *38*, 1426–1435.

84 D. Bikiaris, *Materials* **2010**, *3*, 2884–2946.

85 T. Chatterjee, K. Yurekli, V. G. Hadjiev, R. Krishnamoorti, *Adv. Funct. Mater.* **2005**, *15*, 1832–1838.

86 J. N. Coleman, U. Khan, W. J. Blau, Y. K. Gun'ko, *Carbon* **2006**, *44*, 1624–1652.

87 X. Gong, J. Liu, S. Baskaran, R. D. Voise, J. S. Young, *Chem. Mater.* **2000**, *12*, 1049–1052.

88 Y. Liu, S. Kumar, *ACS Appl. Mater. Interfaces* **2014**, *6*, 6069–6087.

89 C. A. Mitchell, J. L. Bahr, S. Arepalli, J. M. Tour, R. Krishnamoorti, *Macromolecules* **2002**, *35*, 8825–8830.

90 M. Rahmat, P. Hubert, *Compos. Sci. Technol.* **2011**, *72*, 72–84.

91 J. F. Vega, Y. da Silva, E. Vicente-Alique, R. Núñez-Ramírez, M. Trujillo, M. L. Arnal, A. J. Müller, P. Dubois, J. Martínez-Salazar, *Macromolecules* **2014**, *47*, 5668–5681.

92 X.-L. Xie, Y.-W. Mai, X.-P. Zhou, *Mater. Sci. Eng. R. Rep.* **2005**, *49*, 89–112.

93 A. Malkin, V. Kulichikhin, S. Ilyin, *Rheol. Acta* **2017**, *56*, 177–188.

94 R. M. L. Evans, M. Tassieri, D. Auhl, T. A. Waigh, *Phys. Rev. E* **2009**, *80*, 012501.

95 C. He, P. Wood-Adams, J. M. Dealy, *J. Rheol.* **2004**, *48*, 711–724.

96 F. R. Schwarzl, *Rheol. Acta* **1969**, *8*, 6–17.

97 P. A. Rodgers, *J. Appl. Polym. Sci.* **1993**, *48*, 1061–1080.

98 S. H. Kim, G. W. Mulholland, M. R. Zachariah, *Carbon* **2009**, *47*, 1297–1302.

99 M. Sahimi, *Applications of Percolation Theory*; Taylor & Francis: London, **1993**.

100 D. Stauffer, A. Aharony, *Introduction to Percolation Theory*; Taylor & Francis: London, **2003**.

101 N. Noroozi, J. A. Thomson, N. Noroozi, L. L. Schafer, S. G. Hatzikiriakos, *Rheol. Acta* **2012**, *51*, 179–192.

102 S. B. Kharchenko, J. F. Douglas, J. Obrzut, E. A. Grulke, K. B. Migler, *Nat. Mat.* **2004**, *3*, 564–568.

103 J. F. Vega, J. Martínez-Salazar, M. Trujillo, M. L. Arnal, A. J. Müller, S. Bredeau, P. Dubois, *Macromolecules* **2009**, *42*, 4719–4727.